EUROPEAN ORGANISATION FOR NUCLEAR RESEARCH

CERN-PPE/93-156
24 August 1993

Measurement of the Photon Structure Function F_2^γ in the Reaction $e^+e^- \to e^+e^- +$ hadrons at LEP

Abstract

We present measurements of the hadronic photon structure function $F_2^\gamma(x)$, in two Q^2 ranges with mean values of 5.9 GeV^2 and 14.7 GeV^2. The data were taken by the OPAL experiment at LEP, with $\sqrt{s}$ close to the Z^0 mass and correspond to an integrated e^+e^- luminosity of 44.8 pb^{-1}. In the context of a QCD-based model we find the quark transverse momentum cutoff separating the vector meson dominance (VMD) and perturbative QCD regions to be 0.27 ± 0.10 GeV. We confirm that there is a significant pointlike component of the photon when the probe photon has $Q^2 > 4$ GeV^2. Our measurements extend to lower values of x than any previous experiment, and no increase of $F_2^\gamma(x)$ is observed.

The OPAL Collaboration

R. Akers[16], G. Alexander[23], J. Allison[16], K.J. Anderson[9], S. Arcelli[2], A. Astbury[28], D. Axen[29], G. Azuelos[18,a], J.T.M. Baines[16], A.H. Ball[17], J. Banks[16], R.J. Barlow[16], S. Barnett[16], R. Bartoldus[3], J.R. Batley[5], G. Beaudoin[18], A. Beck[23], G.A. Beck[13], J. Becker[10], C. Beeston[16], T. Behnke[27], K.W. Bell[20], G. Bella[23], P. Bentkowski[18], P. Berlich[10], S. Bethke[11], O. Biebel[3], I.J. Bloodworth[1], P. Bock[11], B. Boden[3], H.M. Bosch[11], M. Boutemeur[18], H. Breuker[8,b], P. Bright-Thomas[25], R.M. Brown[20], A. Buijs[8], H.J. Burckhart[8], C. Burgard[27], P. Capiluppi[2], R.K. Carnegie[6], A.A. Carter[13], J.R. Carter[5], C.Y. Chang[17], D.G. Charlton[8], S.L. Chu[4], P.E.L. Clarke[15], J.C. Clayton[1], I. Cohen[23], J.E. Conboy[15], M. Cooper[22], M. Coupland[14], M. Cuffiani[2], S. Dado[22], G.M. Dallavalle[2], S. De Jong[13], L.A. del Pozo[5], H. Deng[17], A. Dieckmann[11], M. Dittmar[4], M.S. Dixit[7], E. do Couto e Silva[12], J.E. Duboscq[8], E. Duchovni[26], G. Duckeck[11], I.P. Duerdoth[16], D.J.P. Dumas[6], P.A. Elcombe[5], P.G. Estabrooks[6], E. Etzion[23], H.G. Evans[9], F. Fabbri[2], B. Fabbro[21], M. Fierro[2], M. Fincke-Keeler[28], H.M. Fischer[3], D.G. Fong[17], M. Foucher[17], A. Gaidot[21], J.W. Gary[4], J. Gascon[18], N.I. Geddes[20], C. Geich-Gimbel[3], S.W. Gensler[9], F.X. Gentit[21], G. Giacomelli[2], R. Giacomelli[2], V. Gibson[5], W.R. Gibson[13], J.D. Gillies[20], J. Goldberg[22], D.M. Gingrich[30,a], M.J. Goodrick[5], W. Gorn[4], C. Grandi[2], F.C. Grant[5], J. Hagemann[27], G.G. Hanson[12], M. Hansroul[8], C.K. Hargrove[7], P.F. Harrison[13], J. Hart[8], P.M. Hattersley[1], M. Hauschild[8], C.M. Hawkes[8], E. Heflin[4], R.J. Hemingway[6], G. Herten[10], R.D. Heuer[8], J.C. Hill[5], S.J. Hillier[8], T. Hilse[10], D.A. Hinshaw[18], J.D. Hobbs[8], P.R. Hobson[25], D. Hochman[26], R.J. Homer[1], A.K. Honma[28,a], R.E. Hughes-Jones[16], R. Humbert[10], P. Igo-Kemenes[11], H. Ihssen[11], D.C. Imrie[25], A.C. Janissen[6], A. Jawahery[17], P.W. Jeffreys[20], H. Jeremie[18], M. Jimack[1], M. Jones[29], R.W.L. Jones[8], P. Jovanovic[1], C. Jui[4], D. Karlen[6], K. Kawagoe[24], T. Kawamoto[24], R.K. Keeler[28], R.G. Kellogg[17], B.W. Kennedy[15], J. King[13], S. Kluth[5], T. Kobayashi[24], D.S. Koetke[8], T.P. Kokott[3], S. Komamiya[24], J.F. Kral[8], R. Kowalewski[8], J. von Krogh[11], J. Kroll[9], P. Kyberd[13], G.D. Lafferty[16], H. Lafoux[21], R. Lahmann[17], J. Lauber[8], J.G. Layter[4], P. Leblanc[18], A.M. Lee[31], E. Lefebvre[18], M.H. Lehto[15], D. Lellouch[26], C. Leroy[18], J. Letts[4], L. Levinson[26], S.L. Lloyd[13], F.K. Loebinger[16], J.M. Lorah[17], B. Lorazo[18], M.J. Losty[7], X.C. Lou[12], J. Ludwig[10], A. Luig[10], M. Mannelli[8], S. Marcellini[2], C. Markus[3], A.J. Martin[13], J.P. Martin[18], T. Mashimo[24], P. Mättig[3], U. Maur[3], J. McKenna[29], T.J. McMahon[1], J.R. McNutt[25], F. Meijers[8], D. Menszner[11], F.S. Merritt[9], H. Mes[7], A. Michelini[8], R.P. Middleton[20], G. Mikenberg[26], J. Mildenberger[6], D.J. Miller[15], R. Mir[12], W. Mohr[10], C. Moisan[18], A. Montanari[2], T. Mori[24], M. Morii[24], U. Müller[3], B. Nellen[3], H.H. Nguyen[9], S.W. O'Neale[1], F.G. Oakham[7], F. Odorici[2], H.O. Ogren[12], C.J. Oram[28,a], M.J. Oreglia[9], S. Orito[24], J.P. Pansart[21], B. Panzer-Steindel[8], P. Paschievici[26], G.N. Patrick[20], N. Paz-Jaoshvili[23], M.J. Pearce[1], P. Pfister[10], J.E. Pilcher[9], J. Pinfold[30], D. Pitman[28], D.E. Plane[8], P. Poffenberger[28], B. Poli[2], T.W. Pritchard[13], H. Przysiezniak[18], G. Quast[27], M.W. Redmond[8], D.L. Rees[8], G.E. Richards[16], M. Rison[5], S.A. Robins[5], D. Robinson[8], A. Rollnik[3], J.M. Roney[28], E. Ros[8], S. Rossberg[10], A.M. Rossi[2], M. Rosvick[28], P. Routenburg[30], K. Runge[10], O. Runolfsson[8], D.R. Rust[12], M. Sasaki[24], C. Sbarra[2], A.D. Schaile[26], O. Schaile[10], W. Schappert[6], F. Scharf[3], P. Scharff-Hansen[8], P. Schenk[4], B. Schmitt[3], H. von der Schmitt[11], M. Schröder[12], C. Schwick[27], J. Schwiening[3], W.G. Scott[20], M. Settles[12], T.G. Shears[5], B.C. Shen[4], C.H. Shepherd-Themistocleous[7], P. Sherwood[15], G.P. Siroli[2], A. Skillman[16], A. Skuja[17], A.M. Smith[8], T.J. Smith[28], G.A. Snow[17], R. Sobie[28], R.W. Springer[17], M. Sproston[20], A. Stahl[3], C. Stegmann[10], K. Stephens[16], J. Steuerer[28], R. Ströhmer[11], D. Strom[19], H. Takeda[24], T. Takeshita[24,c], S. Tarem[26], M. Tecchio[9], P. Teixeira-Dias[11],

N. Tesch[3], M.A. Thomson[15], E. Torrente-Lujan[22], S. Towers[28], G. Transtromer[25], N.J. Tresilian[16], T. Tsukamoto[24], M.F. Turner[8], D. Van den plas[18], R. Van Kooten[27], G.J. VanDalen[4], G. Vasseur[21], A. Wagner[27], D.L. Wagner[9], C. Wahl[10], C.P. Ward[5], D.R. Ward[5], P.M. Watkins[1], A.T. Watson[1], N.K. Watson[8], M. Weber[11], P. Weber[6], P.S. Wells[8], N. Wermes[3], M.A. Whalley[1], B. Wilkens[10], G.W. Wilson[4], J.A. Wilson[1], V-H. Winterer[10], T. Wlodek[26], G. Wolf[26], S. Wotton[11], T.R. Wyatt[16], R. Yaari[26], A. Yeaman[13], G. Yekutieli[26], M. Yurko[18], W. Zeuner[8], G.T. Zorn[17].

[1]School of Physics and Space Research, University of Birmingham, Birmingham, B15 2TT, UK
[2]Dipartimento di Fisica dell' Università di Bologna and INFN, Bologna, 40126, Italy
[3]Physikalisches Institut, Universität Bonn, D-5300 Bonn 1, Germany
[4]Department of Physics, University of California, Riverside, CA 92521 USA
[5]Cavendish Laboratory, Cambridge, CB3 0HE, UK
[6]Carleton University, Dept of Physics, Colonel By Drive, Ottawa, Ontario K1S 5B6, Canada
[7]Centre for Research in Particle Physics, Carleton University, Ottawa, Ontario K1S 5B6, Canada
[8]CERN, European Organisation for Particle Physics, 1211 Geneva 23, Switzerland
[9]Enrico Fermi Institute and Dept of Physics, University of Chicago, Chicago Illinois 60637, USA
[10]Fakultät für Physik, Albert Ludwigs Universität, D-7800 Freiburg, Germany
[11]Physikalisches Institut, Universität Heidelberg, Heidelberg, Germany
[12]Indiana University, Dept of Physics, Swain Hall West 117, Bloomington, Indiana 47405, USA
[13]Queen Mary and Westfield College, University of London, London, E1 4NS, UK
[14]Birkbeck College, London, WC1E 7HV, UK
[15]University College London, London, WC1E 6BT, UK
[16]Department of Physics, Schuster Laboratory, The University, Manchester, M13 9PL, UK
[17]Department of Physics, University of Maryland, College Park, Maryland 20742, USA
[18]Laboratoire de Physique Nucléaire, Université de Montréal, Montréal, Quebec, H3C 3J7, Canada
[19]University of Oregon, Dept of Physics, Eugene, Oregon 97403, USA
[20]Rutherford Appleton Laboratory, Chilton, Didcot, Oxfordshire, OX11 0QX, UK
[21]DAPNIA/SPP, Saclay, F-91191 Gif-sur-Yvette, France
[22]Department of Physics, Technion-Israel Institute of Technology, Haifa 32000, Israel
[23]Department of Physics and Astronomy, Tel Aviv University, Tel Aviv 69978, Israel
[24]International Centre for Elementary Particle Physics and Dept of Physics, University of Tokyo, Tokyo 113, and Kobe University, Kobe 657, Japan
[25]Brunel University, Uxbridge, Middlesex, UB8 3PH UK
[26]Nuclear Physics Department, Weizmann Institute of Science, Rehovot, 76100, Israel
[27]Universität Hamburg/DESY, II Inst für Experimental Physik, Notkestrasse 85, 22607 Hamburg, Germany
[28]University of Victoria, Dept of Physics, P O Box 3055, Victoria BC V8W 3P6, Canada
[29]University of British Columbia, Dept of Physics, Vancouver BC V6T 1Z1, Canada
[30]University of Alberta, Dept of Physics, Edmonton AB T6G 2N5, Canada
[31]Duke University, Dept of Physics, Durham, North Carolina 27708-0305, USA

[a]Also at TRIUMF, Vancouver, Canada V6T 2A3

[b]Now at MPI, München, Germany
[c]Also at Shinshu University, Matsumoto 390, Japan

1 Introduction

This paper reports measurements of the F_2^γ hadronic structure function of the photon at intermediate Q^2 ($4 < Q^2 < 30$ GeV^2) using data taken by the OPAL experiment at LEP in the period 1990-1992. The data sample corresponds to an integrated e^+e^- luminosity of 44.8 pb^{-1}. The analysis uses singly-tagged events, with the tagged $e^\pm$ detected at angles between 47 and 120 mrad to the beam direction.

Witten's original proposal [1] that F_2^γ would evolve with Q^2 according to perturbative QCD has been confirmed by experiments at lower energy e^+e^- colliders which [2-9] have measured $F_2^\gamma(x)$ with $<Q^2>$ ranging from 0.1 GeV^2 to 500 GeV^2. However, the use of that evolution to extract an unambiguous value for the scale parameter $\Lambda_{\overline{MS}}$ has been plagued with theoretical uncertainties [10-14].

The TPC/2γ experiment [2] demonstrated that at low Q^2 (< 1.5 GeV^2) the target photon behaves like a vector meson, with the x dependence of F_2^γ agreeing well with the pion structure function as studied in Drell Yan processes [15]; as an S-wave state, the π is expected to be a good model for the ρ structure function [16].

A number of experiments with data at a mean Q^2 of ~ 5 GeV^2 [3, 4] show that $F_2^\gamma(x)$ begins to grow for $x > 0.3$, as predicted by QCD, but the transformation from $Q^2 \sim 1$ GeV^2 to $Q^2 \sim 5$ GeV^2 is so abrupt that it has been difficult to devise a model which fits both regions [17-20]. The OPAL data reported here confirm previous results on the upper side of this abrupt transformation.

2 The Opal Detector

The OPAL detector, described in detail elsewhere [21], has a uniform solenoidal magnetic field of 0.4 T throughout the central tracking region, with electromagnetic and hadronic calorimetry outside the coil. For this analysis the most important sub-detectors are the Forward Detectors, the Central Jet and Vertex Chambers which trigger on and measure charged tracks, and the lead-glass Electromagnetic Barrel and Endcap Calorimeters.

The Forward Detectors are used to tag leptons which have made deep-inelastic scatters with nearly-real photons radiated by particles in the opposing beam (see discussion in Section 3). These detectors, which cover the small-angle region at each end of OPAL, consist of cylindrical lead-scintillator calorimeters with a depth of 24 radiation lengths (X_0) divided azimuthally into 16 segments. The energy resolution is $18\%/\sqrt{E}$, where E is in GeV. Positional information is derived from the energy sharing between adjacent segments, and by the sharing of light between the inner and outer edges of each segment. An array of three planes of proportional tubes buried

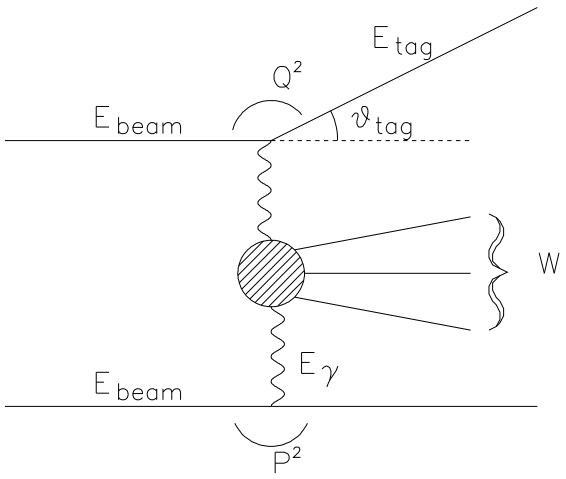

Figure 1: The multiperipheral two-photon process.

in the calorimeter at a depth of $4X_0$ provides a better shower position measurement, with a typical resolution of 3-4 mm, corresponding to 2.5 mrad in the polar angle ϑ, and less than 3.5 mrad in the azimuthal angle ϕ. The clear acceptance of the Forward Detectors covers the angular range from 47 to 120 mrad from the beam direction.

3 Kinematics

The cross section for deep inelastic scattering of an $e^{\pm}$ from a nearly real virtual photon associated with the opposing $e^{\mp}$ can be written in terms of the structure functions $F_1^\gamma(x,Q^2)$ and $F_2^\gamma(x,Q^2)$ as [22]

$$\frac{d^2\sigma}{dxdy} = \frac{16\pi\alpha^2 E_{beam}E_\gamma}{Q^4}[(1-y)F_2^\gamma(x,Q^2) + xy^2F_1^\gamma(x,Q^2)] \tag{1}$$

where the kinematic variables are defined with reference to Figure 1. E_{beam} is the incoming beam energy and E_γ the energy of the target photon. Q^2, x, and y are given by

$$Q^2 = 2E_{beam}E_{tag}(1-\cos\vartheta_{tag}), \tag{2}$$

$$x = \frac{Q^2}{Q^2+W^2}, \tag{3}$$

$$y = 1 - \frac{E_{tag}}{E_{beam}}\cos^2(\vartheta_{tag}/2), \tag{4}$$

where E_{tag} is the energy of the tagged $e^{\pm}$ and ϑ_{tag} is its angle to the beam direction. W is the invariant mass of the two-photon system which gives rise to the final-state hadrons in this analysis. Because of the loss of particles near the beam pipe, W is not directly measurable. We define W_{trk} to be the invariant mass of the charged tracks, while W_{vis} is the mass of all of the hadrons seen in the detector. The quantities x_{trk} and x_{vis} are defined by adding the appropriate subscripts to (3). In testing the Monte Carlo program (see Section 5 below), we also use the variable P^2, the four-momentum transfer squared to the untagged lepton, defined analogously to Q^2. In the kinematic region considered here, $y \ll 1$, so that the second term in (1) is much smaller than the first and the measured cross section is effectively proportional to $F_2^{\gamma}(x, Q^2)$.

4 Event Selection Criteria

The event selection cuts require a high-energy cluster (the tag) in the Forward Detector, in association with charged tracks detected in the Central Detectors. The selection cuts are summarised in Table 1, and are discussed in more detail in this section.

The measured energy must be at least $0.775 \times E_{beam}$, to exclude backgrounds arising from multihadronic Z^0 decays, and from untagged two-photon events coincidentally associated with fake tags caused by off-momentum beam particles. Figure 2 shows the distribution of events in E_{tag}/E_{beam} and the normalised transverse momentum k_T, defined by

$$k_T = ({p_T}^{tag} + {p_T}^{vis})/{p_T}^{tag}.$$

Here ${p_T}^{tag}$ is the transverse momentum of the tagged lepton with respect to the beam axis, and ${p_T}^{vis}$ is the component of the total transverse momentum of the other observed particles in the plane defined by the beam and the tagged lepton (the "tag plane"). In this plane, ${p_T}^{tag}$ defines the positive direction, while ${p_T}^{vis}$ can have either sign. The events plotted pass all of our selection cuts, except that no tag energy or transverse momentum cuts have been applied. The tagged two-photon signal is represented by the cluster of events centred close to $k_T = 0$ which is visible at high E_{tag}/E_{beam}; the background events appear at lower E_{tag}/E_{beam}, and have a much flatter distribution in k_T.

In addition to the tag energy cut,we restrict the measured angle of the tag cluster to ensure that the shower is completely contained in the Forward Detector. Events where both leptons are detected at large angles are rejected, to ensure that the target photon is close to the mass shell.

Only events having at least three reconstructed charged tracks are accepted. We demand that W_{vis} be greater than 2.5 GeV, so that the accepted events are well above the hadronic resonance region, and make cuts on the transverse momentum of the charged tracks, both in and out of the tag plane.

A total of 1350 events pass all of the cuts, of which 555 have $Q^2 < 8$ GeV^2, and 795 have $Q^2 > 8$ GeV^2. The distribution of these events in the $x_{vis} - Q^2$ plane is shown in Figure 3.

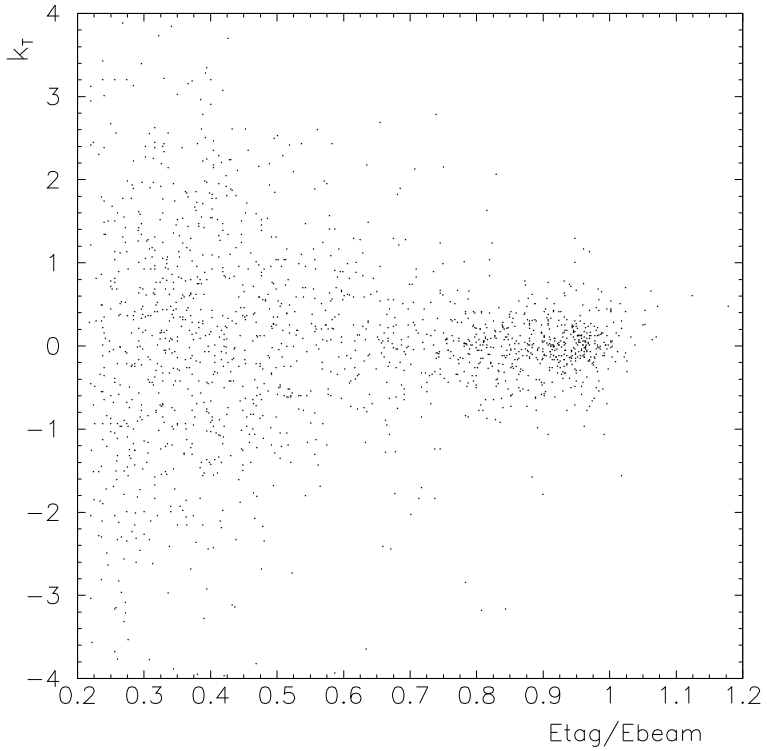

Figure 2: Distribution of events in scaled transverse momentum k_T and E_{tag}/E_{beam}.

Several independent calorimetric and track-based triggers contribute to the final event sample. The resulting redundancy enables us to determine the overall trigger efficiency to be $99.0 \pm 0.2\%$.

5 Monte Carlo Simulation

Many of the hadrons in tagged two-photon events are produced at small angles to the incoming e^+e^- beam axis, and remain undetected in the beam pipe. Consequently, it is important that the Monte Carlo model accurately represents the data and the detector, to permit the effects of finite detector acceptance and resolution to be unfolded (see Section 8.1). The OPAL detector simulation program is described in detail elsewhere [23]. This section describes the event generators used in this analysis.

We use a new Monte Carlo program TWOGEN [24] to generate events according to chosen formulae for $F_2^\gamma(x, Q^2, P^2)$ or $F_2^\gamma(x, Q^2)$. TWOGEN is based on the transverse-transverse two-photon luminosity generator developed by Langeveld [25] for analysis of two-photon data from the TPC/2γ experiment. A quark-antiquark state is generated with mass W and a quark-parton model (QPM) angular distribution in the two-photon centre of mass, and is allowed to fragment by using the Lund string model [26, 27].

As a check, TWOGEN has been compared with the predictions of the QED matrix-element

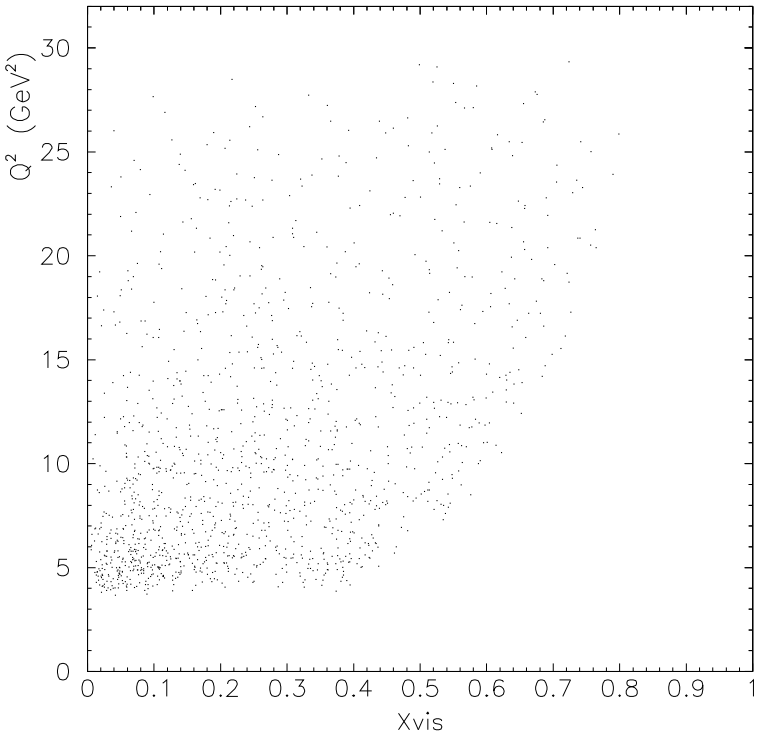

Figure 3: Distribution of selected events in x_{vis} and Q^2.

Monte Carlo program of Vermaseren [28, 29, 30], with quark masses, charges and colours set to reproduce QPM. For the purposes of this comparison, we used the QPM formula for $F_2^\gamma(x, Q^2, P^2)$ [31]. The two programs agree to within 1.4% in overall normalization, which is assigned as a systematic error in the normalization of the unfolded structure function.

In generating samples for comparison with the data a number of contributions must be combined.

a) QCD. There are numerous formulae which could be used in TWOGEN. We have chosen the "all order QCD" approach of Kapusta et al. [12, 13, 32], as parametrized in [9], with the QCD scale parameter Λ taken to be 200 MeV. The change in the behaviour of the structure function at Q^2 close to 1 GeV^2 is built into this model by setting a cutoff in p_t, the transverse momentum of the virtual quark with respect to the photon axis in the two-photon centre-of-mass frame. The pointlike behaviour of the QCD formula is assumed to apply to all $p_t > p_t^0$, but a separate part must be added to the cross section to allow for the hadron-like behaviour of the target photon for $p_t < p_t^0$. This extra contribution is parametrized by the Vector Meson Dominance model.

b) VMD. The Vector Meson Dominance contribution is calculated using the TWOGEN Monte Carlo with a structure function formula which has been shown to fit data at $Q^2 < 1$ GeV^2 [2, 3]. We have verified that our results do not change significantly if we use the simpler expression $F_2^\gamma(x)/\alpha = 0.2(1-x)$ [22] instead. Following [2, 3], we consider two VMD models, with different angular distributions of the quark-antiquark axis in the two-photon centre-of-

Charged Track Quality	Closest approach in $(x, y) < 2.5$ cm from beam Closest approach in $z < 10$ cm from interaction point At least 20 hits in Jet chamber Radius of first hit < 75 cm $\lvert\cos\vartheta\rvert < 0.97$ $p_T > 0.1$GeV
Electromagnetic Cluster Quality	$E_{raw} > 0.17$ GeV Cluster is not associated with a track (association half-angle $\eta = 0.1$ rad)
Track Multiplicity	≥ 3 charged tracks *of which* ≥ 1 with $p_T > 1$ GeV *and* ≥ 1 other with $p_T > 0.5$ GeV
Tag Antitag	$E_{tag} > 0.775 \times E_{beam}$ $47 < \vartheta_{tag} < 120$ mrad No electromagnetic cluster with energy $E_{clus} > 0.25 \times E_{beam}$ in hemisphere opposite tag
p_T balance	$\lvert {p_T}_{in}^{vis} + {p_T}^{tag}\rvert < 6$ GeV (in tag plane) $\lvert {p_T}_{out}^{vis}\rvert < 4$ GeV (out of tag plane)
Hadronic mass	2.5 GeV $< W_{vis} <$ 40 GeV

Table 1: Event selection requirements

mass frame. The weight given to each model in our final Monte Carlo sample is adjusted to achieve the best fit to the data (cf. Section 7.1). In model A (VMD "peripheral"), we generate the angular distribution according to an exponential distribution of quark transverse momentum with a mean of 300 MeV with respect to the photon axis. Model B produces the angular distribution of QED fermion pair production by real photons. We generated this sample using the same VMD structure function as in model A, followed by a sampling from the same "fermion pair" quark angular distribution as was used for the QCD events.

c) Charmed quark and tau lepton production. Events in both of these channels are generated with the Vermaseren Monte Carlo, i.e. assuming that the heavy quark behaves according to QPM at these modest Q^2 values, and that the tau lepton behaves according to QED.

Events from all five Monte Carlo samples (QCD, VMD model A, VMD model B, charm-anticharm and tau-antitau) are passed through the OPAL simulation program [23] and recon-

structed in the same way as real data. They are then analysed with the same selection criteria as the real sample. The number of events in each category passing all of the two-photon selection cuts is given in Table 2. The total sample generated corresponded to approximately five times our actual integrated e^+e^- luminosity; the figures in the table have been normalized to 44.8 pb^{-1}.

Generator	QCD	VMD	$c\overline{c}$	$\tau^+\tau^-$
Normalized number of events	808	325	178	64

Table 2: Monte Carlo events by Category. The QCD events were simulated with $p_t^0 = 0.27$ GeV.

We have corrected for the finite range of target-photon masses allowed by our antitagging cut by comparing a sample of Monte Carlo events from the TWOGEN program using the P^2-dependent version of the QPM formula for F_2^γ [31] with a sample generated using a P^2-independent QPM formula [1]. The cross section within our acceptance is 5% smaller when integrated over the accepted range of P^2, as compared to the calculation with $P^2 = 0$. There is also a small change in the shape of the x distribution. These corrections are only applied to the QCD component of the Monte Carlo as it is not obvious that this comparison, calculated from the quark parton model, should apply to the VMD component of our data. The $c\overline{c}$ and $\tau^+\tau^-$ components generated with the Vermaseren program already include a P^2 dependence.

6 Estimation of Backgrounds

In addition to the $e^+e^-\tau^+\tau^-$ final state mentioned above, the following processes give rise to background events.

6.1 $e^+e^- \rightarrow$ hadrons

There is a small probability that a hadronic Z^0 decay could satisfy the two-photon selection criteria. The resonant enhancement at the Z^0 peak makes this problem potentially more serious at LEP than at previous e^+e^- colliders. We have investigated this using Monte Carlo events simulated with the Jetset73 package [33]. Our selection cuts reject these events very effectively, giving the background estimates shown in Table 3.

6.2 $e^+e^- \rightarrow \tau^+\tau^-$

As in the hadronic case, tau pairs produced in Z^0 decay can in principle fake tagged two-photon events. An analysis of 72000 such events produced with the KORALZ generator [34]

x bin	Background $4 < Q^2 < 8$ GeV^2	Background $8 < Q^2 < 30$ GeV^2
0.0-0.1	2.0 ± 2.0	5.9 ± 3.4
0.1-0.2	–	2.0 ± 2.0
0.2-0.3	–	2.0 ± 2.0

Table 3: Monte Carlo estimate of multihadronic background.

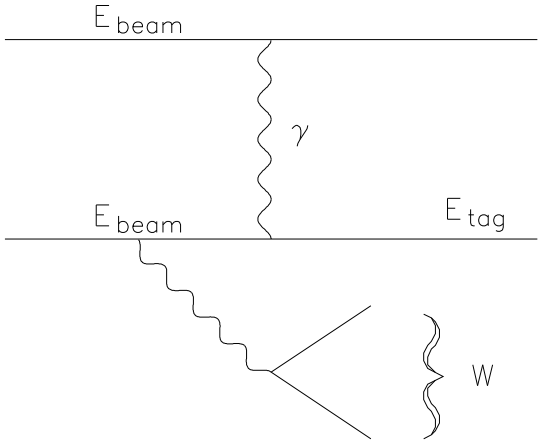

Figure 4: The bremsstrahlung background process.

found no events satisfying our selection cuts. Since this Monte Carlo sample corresponds to an integrated luminosity of approximately 1.2 times that used in this analysis, the background from $Z^0 \to \tau^+\tau^-$ events is expected to be negligible.

6.3 Non-multiperipheral $e^+e^- \to e^+e^-$ + hadrons

There are several processes other than the multiperipheral diagram of Figure 1 which can give rise to the same final state. These processes have been studied using the Monte Carlo generator FERMISV [35], which incorporates both Z^0 and γ exchange diagrams and interference terms. By far the largest contribution arises from the bremsstrahlung, or "inelastic Compton", process shown in Figure 4. The resulting background is estimated as $(0.4 \pm 0.2)\%$ of the multiperipheral cross section, or 5.4 ± 2.7 events, the error being the Monte Carlo statistical uncertainty. The Q^2 distribution of these events follows that of the multiperipheral sample; they are uniformly

distributed in x between the values of 0.2 and 0.7. The effect of interference between the multiperipheral and bremsstrahlung diagrams is found to be much less than the bremsstrahlung cross section and can safely be neglected.

6.4 Beam-gas events

Background events arising from interactions with residual gas in the beam pipe would have their vertex position uniformly distributed along the beam axis. By studying events originating outside our ± 10 cm cut, we estimate that our final sample contains 3.0 ± 0.9 such events. Events in which an off-momentum electron simulates a Forward Detector tag have been studied as part of the OPAL luminosity determination [36, 37]; such events are clustered at low "tag" energies, as shown in Figure 2, and can be neglected at $E_{tag} > 0.775 \times E_{beam}$.

7 Results of the Analysis

7.1 Fit for the QCD cutoff parameter p_t^0.

The transverse momentum cutoff p_t^0 in the QCD model for F_2^γ [12, 13, 32] has been determined by fitting the Monte Carlo x_{vis} distribution to the data (Figures 5 and 6). The Monte Carlo samples from QCD, VMD model A, charm and tau pairs were individually normalized to the observed luminosity, then added together and the backgrounds subtracted, leaving only p_t^0 to be varied.

The results of the fits are given in Table 4. The central values of p_t^0 in the two Q^2 ranges are consistent with the value of 0.27 ± 0.10 obtained by fitting over the whole data set.

Q^2range (GeV^2)	x range	p_t^0 (GeV)	χ^2/DOF
$4 - 8$	$0.001 - 0.649$	0.44 ± 0.20	12.6/5
$8 - 30$	$0.006 - 0.836$	0.19 ± 0.12	6.2/7
$4 - 30$	$0.001 - 0.836$	0.27 ± 0.10	8.2/7

Table 4: Values of p_t^0 measured from the x_{vis} distribution.

In order to test whether a model B component is needed in the VMD Monte Carlo sample, as discussed in Section 5, we examined the event distributions in Q^2, ϑ_{tag}, and $(p_T^{lead})^2$, where p_T^{lead} is the momentum component perpendicular to the tag plane of the hadron with the highest momentum. In each case, the data is best represented when the VMD event sample is 100% model A.

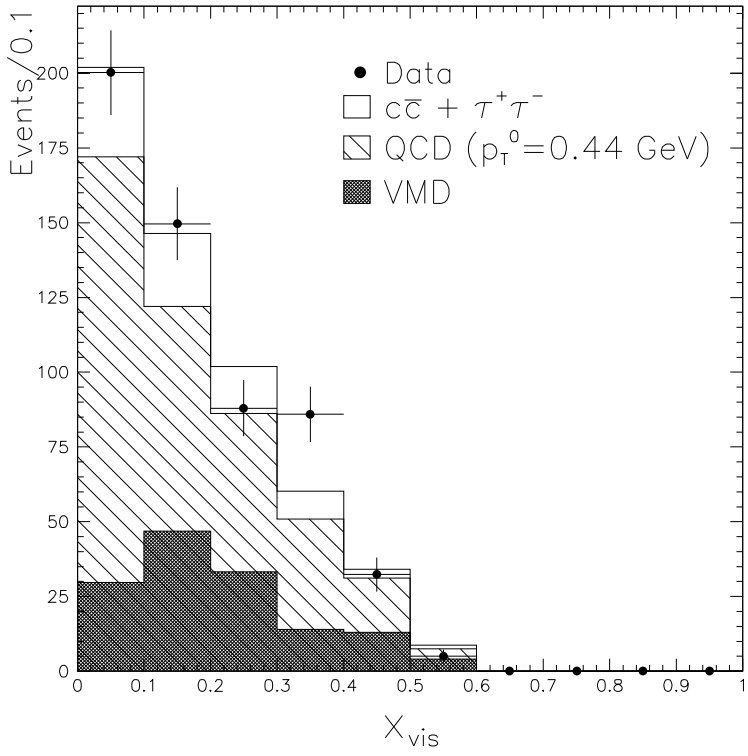

Figure 5: Comparison of data and Monte Carlo x_{vis} distributions, for $4 < Q^2 < 8$ GeV^2. The unshaded part of the histogram represents $\tau^+\tau^-$ and $c\bar{c}$ events.

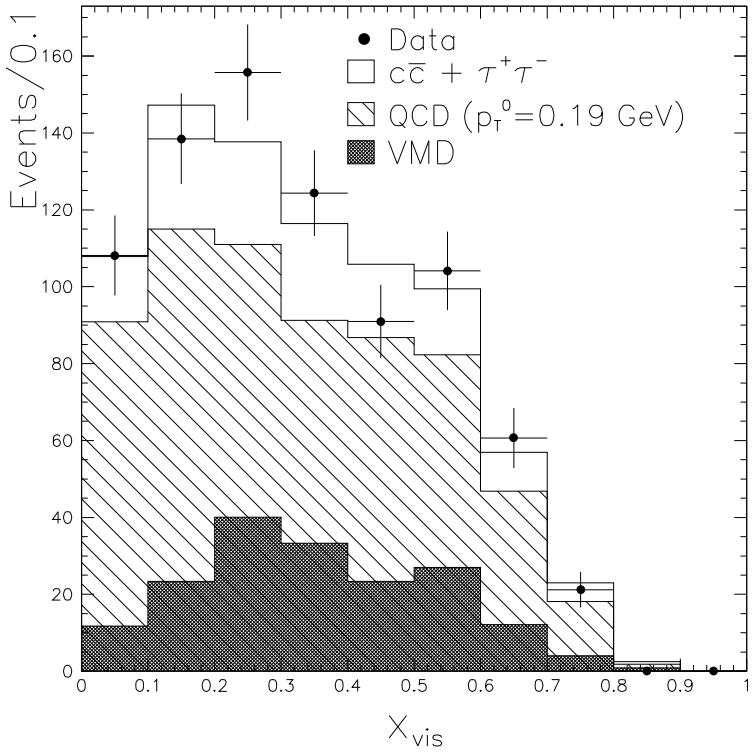

Figure 6: Comparison of data and Monte Carlo x_{vis} distributions, for $8 < Q^2 < 30$ GeV^2. The unshaded part of the histogram represents $\tau^+\tau^-$ and $c\bar{c}$ events.

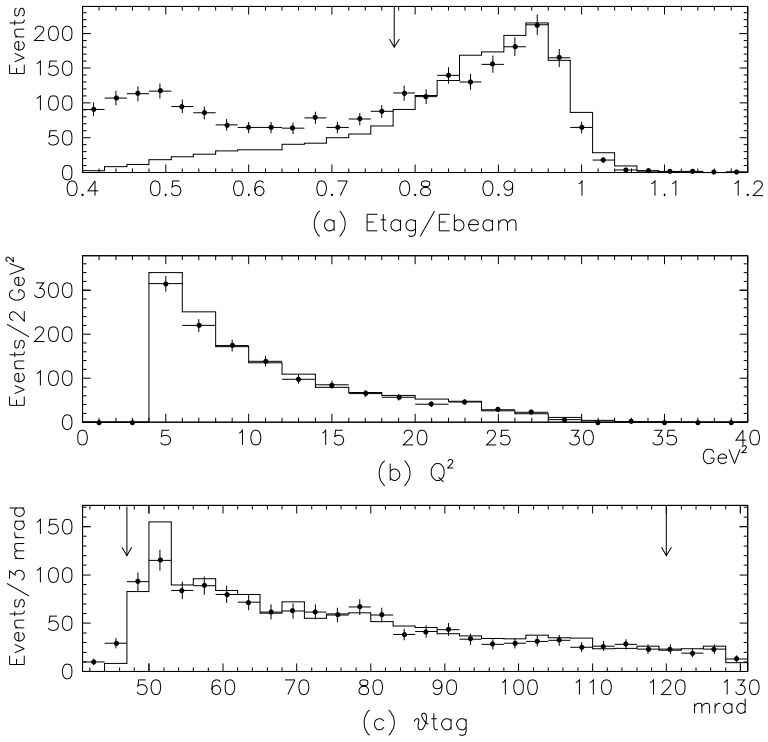

Figure 7: Comparison of data and Monte Carlo tag distributions. The points are the data, and the lines show the Monte Carlo prediction. The arrows represent the selection cuts, detailed in Table 1.

7.2 Comparison of data and Monte Carlo distributions

The event distributions in Q^2, E_{tag}, and ϑ_{tag} (Figure 7) demonstrate that the tagged leptons are reasonably well described by the Monte Carlo with p_t^0 determined as described above. The disagreement between the data and the simulation at low tag energies is principally caused by the classes of background discussed in Section 4 above. The discrepancy at $\vartheta_{tag} \sim 52$ mrad in Figure 7(c) occurs at the edge of the acceptance of the proportional tube counters. This effect is not perfectly modelled by the detector simulation, leading to the depletion of Monte Carlo events at low ϑ_{tag}, compensating for the excess in the 52 mrad bin. In variables of physical interest, in particular x_{vis}, this local imperfection is not significant. Figure 8 shows variables which depend upon the simulation of the hadronic final state. The agreement is acceptable for our purposes. However, there are significant discrepancies in regions of the plots sensitive to the fact that the Lund fragmentation scheme is known not to be reliable for hadron systems with mass W close to the lower cut at 2.5 GeV. The resulting systematic errors are discussed below.

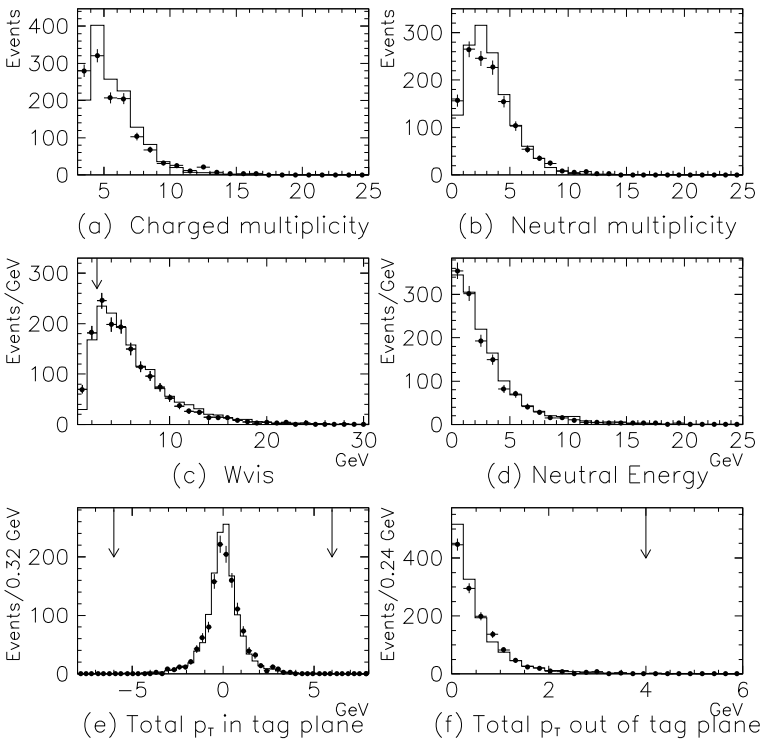

Figure 8: Comparison of data and Monte Carlo hadronic distributions. The points are the data, and the lines show the Monte Carlo prediction. The arrows represent the selection cuts, detailed in Table 1.

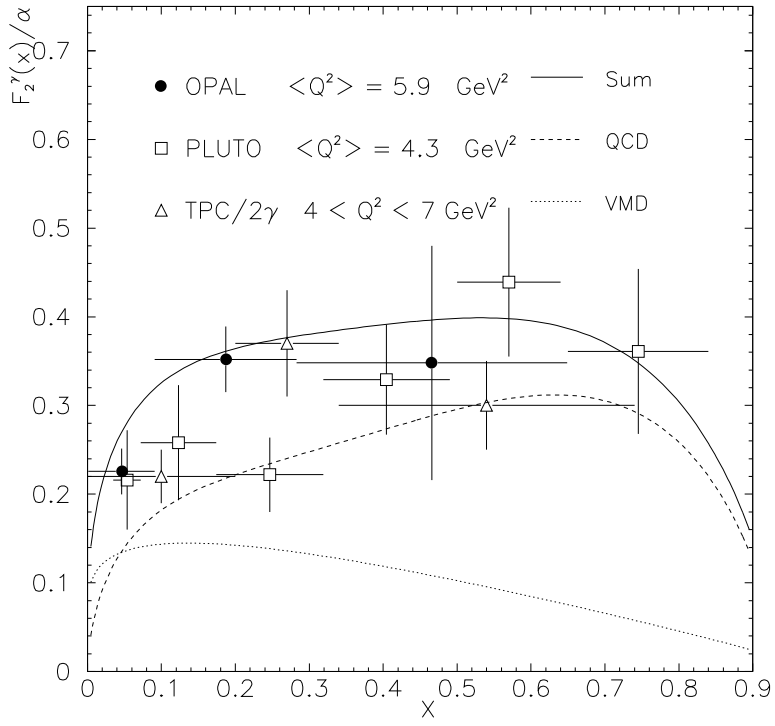

Figure 9: Unfolded $F_2^\gamma(x)$at $<Q^2> = 5.9$ GeV^2, with previous measurements at similar mean Q^2 shown for comparison. The curves show the predictions of a QCD-based model (see text). The error bars give the statistical and systematic errors added in quadrature.

8 Measurement of the F_2^γ structure function

8.1 Unfolding the detector effects

In order to obtain a measurement of F_2^γ which can be compared with theoretical calculations and results from other experiments, we correct for the finite detector acceptance and resolution effects using the unfolding program of Blobel [38] to transform the measured x_{vis} distribution into the estimated $F_2^\gamma(x)$ in true x space. This program avoids the statistical instabilities inherent in the naïve "matrix inversion" technique which can give rise to bin-to-bin correlations and unphysical fluctuations in the unfolded result (see [38] for details). The systematic errors arising from the unfolding procedure are discussed below.

Our unfolded measurements of $F_2^\gamma(x)$ are shown in Figure 9 for the Q^2 region $4 < Q^2 < 8$ GeV^2, and in Figure 10 for $8 < Q^2 < 30$ GeV^2. Also shown for comparison are earlier results obtained by the PLUTO [4] and TPC/2γ [2] collaborations at comparable $<Q^2>$. The curves show the prediction of the QCD model of [12, 13, 32] including the VMD contribution, evaluated for the Q^2 range covered by the OPAL data. Our results are consistent with the other experiments in the respective Q^2 regions and agree well with the model.

The unfolded measurements and associated errors are summarised in Tables 5 and 6. The

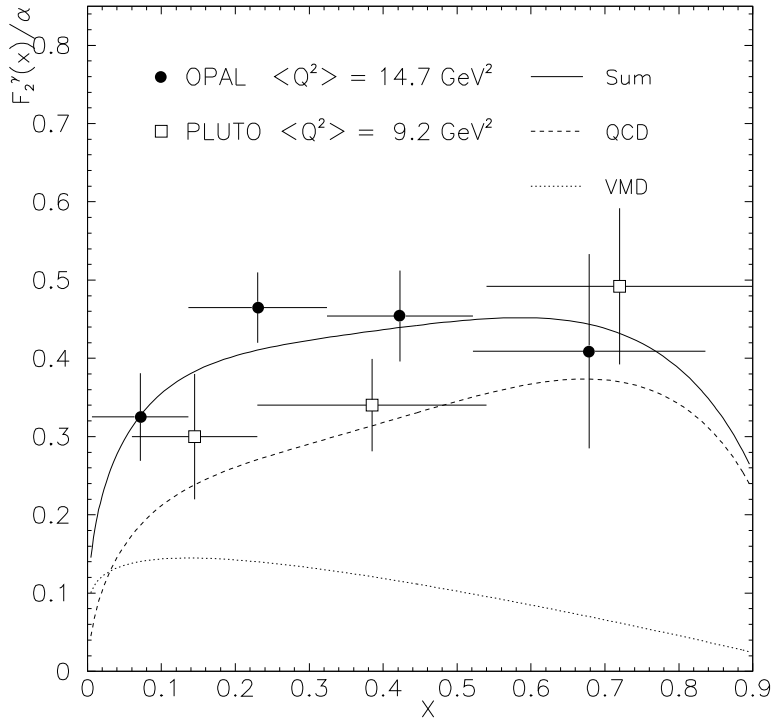

Figure 10: Unfolded $F_2^\gamma(x)$at $<Q^2> = 14.7$ GeV^2, with a previous measurement at similar mean Q^2 shown for comparison. The curves show the predictions of a QCD-based model (see text). The error bars give the statistical and systematic errors added in quadrature.

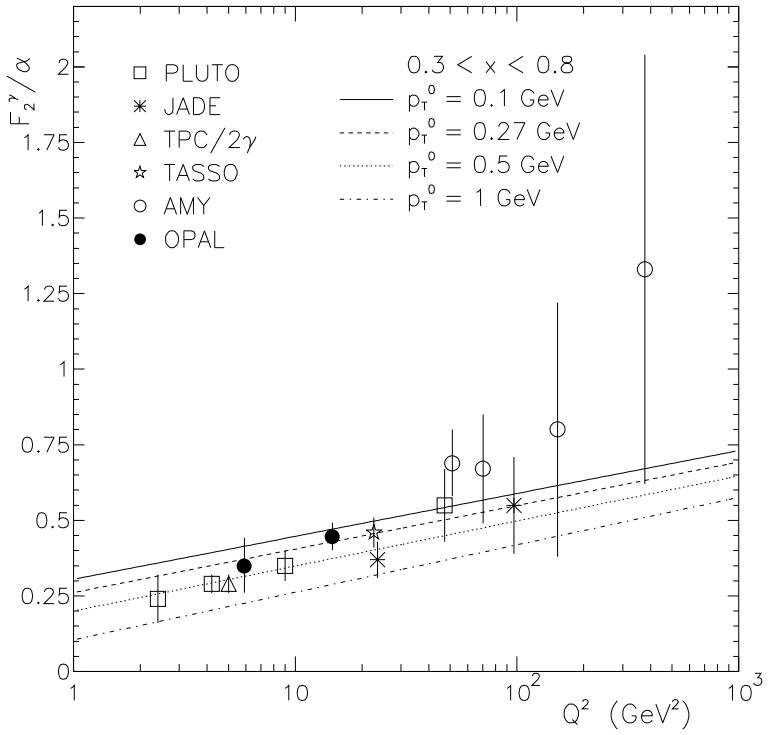

Figure 11: Variation of $< F_2^\gamma(x) >$ with Q^2 (adapted from [9]).

systematic errors shown in the tables are discussed below.

Figure 11 shows the variation in the mean value of F_2^γ/α for $0.3 < x < 0.8$, as a function of Q^2. The lower integration limit ensures that the effect of the VMD contribution is small, while the upper limit is required because the statistical errors increase rapidly in most experiments as $x \to 1$. The present OPAL data points are shown as solid circles. The lines show the predictions of the QCD model of refs [12, 13, 32] for several values of the cutoff parameter p_t^0.

8.2 Systematic errors

Several sources of systematic error have been considered, as follows.

(a) Variation of cuts. We have repeated the analysis with the tag energy cut altered by $\pm 0.025 \times E_{beam}$ and $\pm 0.050 \times E_{beam}$ from its standard value; this represents $1\times$ and $2\times$ the energy resolution of the Forward Detector. Similarly, we have varied the cut on W_{vis} between 2 GeV and 3 GeV in steps of 0.25 GeV, and analysed the data using only charged track information. From the RMS variation of unfolded results a point by point systematic error was assigned as given in Tables 5 and 6. The errors from this source are less than the statistical errors on all points, except for the lowest x point in the upper range of Q^2.

The discrepancy between the charged multiplicity distribution in the data and the prediction of our Monte Carlo model, seen in Figure 8(a), means that the normalization of F_2^γ is sensitive

x range	0.001-0.091	0.091-0.283	0.283-0.649
F_2^γ/α	0.224	0.352	0.348
Statistical error	0.018	0.030	0.090
Variation of cuts	0.018	0.018	0.080
Unfolding error	0.006	0.011	0.053
Overall syst. error	0.019	0.021	0.096
Total error	0.026	0.037	0.132

Table 5: Summary of unfolded $F_2^\gamma(x)$ measurement at $<Q^2> = 5.9$ GeV^2. The x bin limits are chosen by the unfolding package to minimize bin-to-bin correlations. The tabulated errors are not correlated between bins; there is an additional uncertainty of 5.9% on the overall normalization of $F_2^\gamma(x)$ arising from the charged multiplicity cut, the Monte Carlo normalization, and the ISR correction, and the luminosity measurement.

x range	0.006-0.137	0.137-0.324	0.324-0.522	0.522-0.836
F_2^γ/α	0.325	0.465	0.446	0.409
Statistical error	0.029	0.038	0.051	0.102
Variation of cuts	0.048	0.023	0.023	0.065
Unfolding error	0.005	0.009	0.016	0.029
Overall syst. error	0.048	0.025	0.028	0.071
Total error	0.056	0.045	0.058	0.124

Table 6: Summary of unfolded $F_2^\gamma(x)$ measurement at $<Q^2> = 14.7$ GeV^2. The x bin limits are chosen by the unfolding package to minimize bin-to-bin correlations. The tabulated errors are not correlated between bins; there is an additional uncertainty of 5.9% on the overall normalization of $F_2^\gamma(x)$ arising from the charged multiplicity cut, the Monte Carlo normalization, and the ISR correction, and the luminosity measurement.

to the cut on the number of charged tracks. We have studied the variation in the mean value of the unfolded $F_2^\gamma(x)$ as the minimum charged multiplicity varies from 3 to 5 tracks. The RMS variation is 5.4%, which we assign as a systematic error common to all x points.

The measurements of $F_2^\gamma(x)$ are insensitive to variations of the other cuts.

(b) Variation of unfolding parameters. The unfolding procedure handles the data internally in the form of binned histograms. For our main analysis, we chose a bin size giving a mean of approximately 20 events per bin; this required roughly 30 bins in each Q^2 range. The systematic error under the heading of "unfolding" in Tables 5 and 6 has been estimated by repeating the analysis with the number of bins varying between 10 and 60 and calculating the RMS variation of each point of the unfolded structure function. None of the unfolded points is sensitive to such variations, except the high-x point in the low Q^2 region. Even in this case the systematic change is within the statistical error.

(c) Radiative corrections. The TWOGEN Monte Carlo program makes no provision for initial state radiation. Calculations using the FERMISV generator [35] suggest that initial state radiation decreases the cross section for the multiperipheral two-photon process by $(2.7 \pm 1.8)\%$ in comparison to the lowest-order diagram. We therefore decrease the normalization of our measured F_2^γ by this amount, and assign 1.8% as a systematic error.

(d) Monte Carlo systematics. As mentioned above, we estimate a systematic error of 1.4% on the overall normalization of F_2^γ by comparing the TWOGEN Monte Carlo generator with the Vermaseren program. This incorporates the error on the correction for P^2 being non-zero.

(e) Other errors. The precision of the luminosity measurement has been steadily improved, from 0.85% in 1990 to 0.5% in 1992; these errors include theoretical uncertainties in the Bhabha scattering cross section. As most of our data were taken in 1991 and 1992, we assign a systematic error of 0.6% from this source. The 0.2% error on the trigger efficiency is negligible. The effect of backgrounds has been shown to be small; the associated systematic errors have been neglected.

9 Conclusions

We have measured the hadronic photon structure function $F_2^\gamma(x)$ in two ranges of Q^2 with means of 5.9 GeV^2 and 14.7 GeV^2. Our measurements are consistent in shape and absolute normalization with those obtained in previous experiments with similar mean Q^2, and with the predictions of a QCD-based phenomenological model in which a soft hadronic component is added to account for collisions in which the quarks in the target photon have transverse momentum less than approximately 270 MeV. We confirm that a significant pointlike component of the photon is present when the probing photon has $Q^2 > 4$ GeV^2.

Our measurements extend to lower values of x than previous experiments have achieved, particularly in the higher Q^2 range, where we have data below $x = 0.01$. There is no indication that $F_2^\gamma(x)$ increases in this region.

Acknowledgements:

It is a pleasure to thank the SL Division for the efficient operation of the LEP accelerator, the precise information on the absolute energy, and their continuing close cooperation with our experimental group. In addition to the support staff at our own institutions we are pleased to acknowledge the
Department of Energy, USA,
National Science Foundation, USA,
Texas National Research Laboratory Commission, USA,
Science and Engineering Research Council, UK,
Natural Sciences and Engineering Research Council, Canada,
Fussefeld Foundation,
Israeli Ministry of Energy and Ministry of Science,
Minerva Gesellschaft,
Japanese Ministry of Education, Science and Culture (the Monbusho) and a grant under the Monbusho International Science Research Program,
German Israeli Bi-national Science Foundation (GIF),
Direction des Sciences de la Matière du Commissariat à l'Energie Atomique, France,
Bundesministerium für Forschung und Technologie, Germany,
National Research Council of Canada,
A.P. Sloan Foundation, and Junta Nacional de Investigação Científica e Tecnológica, Portugal.

References

[1] E. Witten, Nucl. Phys. B120, (1977) 189.

[2] H. Aihara et al., TPC/2γ Collaboration, Z. Phys. C 34, (1987) 1.

[3] H. Aihara et al., TPC/2γ Collaboration, Phys. Rev. Lett. 58, (1987) 97.

[4] Ch. Berger et al., PLUTO Collaboration, Phys. Lett. 142, (1984) 111.

[5] Ch. Berger et al., PLUTO Collaboration, Nucl. Phys. B281, (1987) 365.

[6] M. Althoff et al., TASSO Collaboration, Z. Phys. C, 31, (1986) 527.

[7] W. Bartel et al., JADE Collaboration, Z. Phys. C, 24, (1984) 231.

[8] H.-J. Behrend et al., CELLO Collaboration, Phys. Lett. 126B, (1983) 391.

[9] T. Sasaki et al., AMY Collaboration, Phys. Lett. B252, (1990) 491.

[10] W. A. Bardeen and A. J. Buras, Phys. Rev. D20, (1979) 166.

[11] D. W. Duke and J. F. Owens, Phys. Rev. D22, (1980) 2280.

[12] J. H. Field, F. Kapusta and L. Poggioli, Phys. Lett. 181B, (1986) 362.

[13] J. H. Field, F. Kapusta and L. Poggioli, Z. Phys. C 36, (1987) 121.

[14] W. R. Frazer, Phys. Lett. B194, (1987) 287.

[15] J. Badier et al., NA3 Collaboration, Z. Phys. C. 18, (1983) 281.

[16] C. Peterson et al., Nucl Phys B174, (1980) 424.

[17] J. H. da Luz Viera and J. K. Storrow, Phys. Lett. B205,(1988) 367.

[18] J. H. da Luz Viera and J. K. Storrow, Phys. Lett. B219, (1989) 529.

[19] J. H. da Luz Viera and J. K. Storrow, Z. Phys. C 51 (1991) 241.

[20] J. Field, P349; Proceedings of VIII International Workshop on Photon-Photon Collisions, Shoresh, Jerusalem Hills, 24-28 April 1988; ed. U. Karshon, World Scientific, Singapore.

[21] K. Ahmet et al., The OPAL Collaboration, Nucl. Inst. Meth. A305, (1991) 275.

[22] H. Kolanoski: "Two Photon Physics at e^+e^- Storage Rings", Springer Verlag (Berlin) 1984.

[23] J. Allison et al., Nucl. Inst. Meth. A317, (1992) 47.

[24] "TWOGEN, a Monte Carlo Generator for Two-Photon Reactions", A. Buijs et al., to be published.

[25] W. G. J. Langeveld, "Pion and Kaon Pair-Production in Photon-Photon Collisions." PhD. thesis, University of Utrecht (1985).

[26] T. Sjöstrand, Comp. Phys. Comm. 47, (1987) 347.

[27] T. Sjöstrand and M. Bengtsson, Comp. Phys. Comm. 43, (1987) 357.

[28] R. Battacharya, G. Grammer Jr., J. Smith, and J.A.M. Vermaseren, Phys. Rev. D15, (1977) 3267.

[29] R. Battacharya, G. Grammer Jr., J. Smith, and J.A.M. Vermaseren, Phys. Rev. D15, (1977) 3280.

[30] R. Battacharya, G. Grammer Jr., J. Smith, and J.A.M. Vermaseren, Phys. Rev. D19, (1979) 137.

[31] C. J. Hill and G. G. Ross, Nucl. Phys. B148, (1979) 373.

[32] F. Kapusta, Z. Phys. C 42, (1989) 225.

[33] T. Sjöstrand, JETSET7.3 Manual, CERN-TH 6488/92.

[34] S. Jadach et al., in Z Physics at LEP, CERN 89-08 Vol 1, eds. G. Altarelli et al. (1989).

[35] J. Hilgart, R. Kleiss, and F. Le Diberder, CERN-PPE/92-115 (1992).

[36] G. Alexander et al., The OPAL Collaboration, Z. Phys. C52 (1991) 175-207.

[37] P. Acton et al., The OPAL Collaboration, Z. Phys. C58 (1993) 219-237.

[38] V. Blobel, in Proceedings of the CERN School of Computing, Aiguablanca, Spain, September 1984, CERN 85-09, ed. C. Verkerk, (1985).